Ceramics International xxx (xxxx) xxx

Contents lists available at ScienceDirect

Ceramics International

journal homepage: www.elsevier.com/locate/ceramint

Crystal structure and optimised microwave dielectric properties of $Ce_2(Zr_{1-x}Ti_x)_3(MoO_4)_9$ solid solutions

Jinjie Zheng [a,b], Yinghao Liu [c], Bingjing Tao [b], Qiang Zhang [b], Haitao Wu [a,*], Xiaoyu Zhang [a,**]

[a] School of Environmental and Material Engineering, Yantai University, Yantai, 264005, Shandong, China
[b] School of Materials Science and Engineering, University of Jinan, Jinan, 250022, Shandong, China
[c] School of Water Conservancy and Environment, University of Jinan, 250022, Jinan, Shandong, China

ARTICLE INFO

Keywords:
Microwave dielectric properties
Crystal structure
$Ce_2(Zr_{1-x}Ti_x)_3(MoO_4)_9$
Far-infrared spectrum

ABSTRACT

$Ce_2(Zr_{1-x}Ti_x)_3(MoO_4)_9$ ($CZ_{1-x}T_xM$) (x = 0.02–0.10) solid solutions were prepared via solid-state reaction method. The effects of Ti^{4+} ions substituting for Zr^{4+} on sintering behavior, structure and microwave dielectric properties of $Ce_2Zr_3(MoO_4)_9$ ceramics were investigated. X-ray diffraction (XRD) patterns combined with Rietveld refinements results confirmed that all compounds crystallized in a trigonal cell (*R-3c*). The *Q·f* values of the as-prepared samples were explained by the packing fraction and average grain size. Dielectric polarizability played a significant role in affecting the permittivity, and the τ_f values were associated with the bond valence of Zr-site. What's more, far-infrared reflectivity spectra were also used to explore the intrinsic dielectric properties of $Ce_2(Zr_{1-x}Ti_x)_3(MoO_4)_9$ (x = 0.08) ceramics. Typically, the desirable microwave dielectric properties of $Ce_2(Zr_{1-x}Ti_x)_3(MoO_4)_9$ ceramics were achieved in x = 0.08 when sintered at 775 °C for 6 h: $\varepsilon_r = 11.28$, $Q{\cdot}f = 84{,}200$ GHz and $\tau_f = -7.86$ ppm/°C.

1. Introduction

With the advent of the 5 G era, there has been a strong interest in the development of microwave devices with high performance [1,2]. Microwave dielectric ceramics with low dielectric constant are vital materials of dielectric substrates that could effectively reduce the electronic signal delay in the millimeter wave (MMW) band, and the ceramics should be equipped with low dielectric loss and excellent frequency stability of temperature, which means high *Q·f* and near-zero τ_f [3–5]. Nowadays, much more research was focus on new findings about microwave dielectric ceramic system [6–11], the improvements on properties by ion substitution [12–15] and the enhancements on temperature stability by preparing composite ceramics [16–18]. Mo-based ceramics, such as $MgMoO_4$, $Na_2Zn_5(MoO_4)_6$, and $[Ca_{0.55}(Nd_{1-x}Bi_x)_{0.3}]MoO_4$ were found to be typical materials with low dielectric constant [19–22]. New double molybdates of lanthanides and transition metal zirconium (Ln_2O_3-ZrO_2-MoO_3 systems) have attracted great attention due to their great technological and scientific significance, and several studies have been focused on the microwave dielectric properties of $Ln_2Zr_3(MoO_4)_9$ (Ln = La, Ce, Nd and Sm) in the past two years [23–28]. Among them, $Ce_2Zr_3(MoO_4)_9$ microwave dielectric ceramics have been reported by Tao et al. and Shi et al., which possessed low sintering temperature (below 800 °C) and outstanding temperature stability ($0 > \tau_f > -10$) [25,26]. Nevertheless, the relatively larger dielectric losses (*Q·f* = 24, 720 GHz) will limit the applications in microwave devices.

Adopting appropriate ion substitution has been an effective strategy for optimizing the dielectric properties [29–31]. For instance, Li et al. improved the quality factor of $CaMgSi_2O_6$ from 59,638 GHz to 83,469 GHz by Mn^{2+} introduction [30]. High *Q·f* value and enhanced dielectric constant were obtained in $Li_2Ti_{0.75}(Mg_{1/3}Nb_{2/3})_{0.25}O_3$ solid solution [31]. Therefore, the substitution of appropriate ions for Zr^{4+} might be an effective way to enhance the microwave dielectric properties of $Ce_2Zr_3(MoO_4)_9$ compounds. It's necessary to utilize suitable cations to substitute Zr^{4+} for lower dielectric loss of $Ce_2Zr_3(MoO_4)_9$ ceramics. Exactly, the ionic radius 0.605 Å of Ti^{4+}(CN = 6) close to that of Zr^{4+}(0.72 Å, CN = 6) [32], and the TiO_2 could improve the microwave dielectric properties in several oxide ceramics by promoting the densification [33]. Consequently, Ti^{4+} was adopted to substitute Zr^{4+} of $Ce_2Zr_3(MoO_4)_9$ in this case.

In this work, $Ce_2(Zr_{1-x}Ti_x)_3(MoO_4)_9$ ($CZ_{1-x}T_xM$) ($0.02 \le x \le 0.1$) ceramics were prepared by solid-state reaction method. The influences of the substitution of Ti^{4+} for Zr^{4+} on phase structure, sinterability and

* Corresponding author.
** Corresponding author.
E-mail addresses: mse_wuht@ujn.edu.cn (H. Wu), zhangxiaoyu@ytu.edu.cn (X. Zhang).

https://doi.org/10.1016/j.ceramint.2020.10.147
Received 8 August 2020; Received in revised form 30 September 2020; Accepted 19 October 2020
Available online 21 October 2020

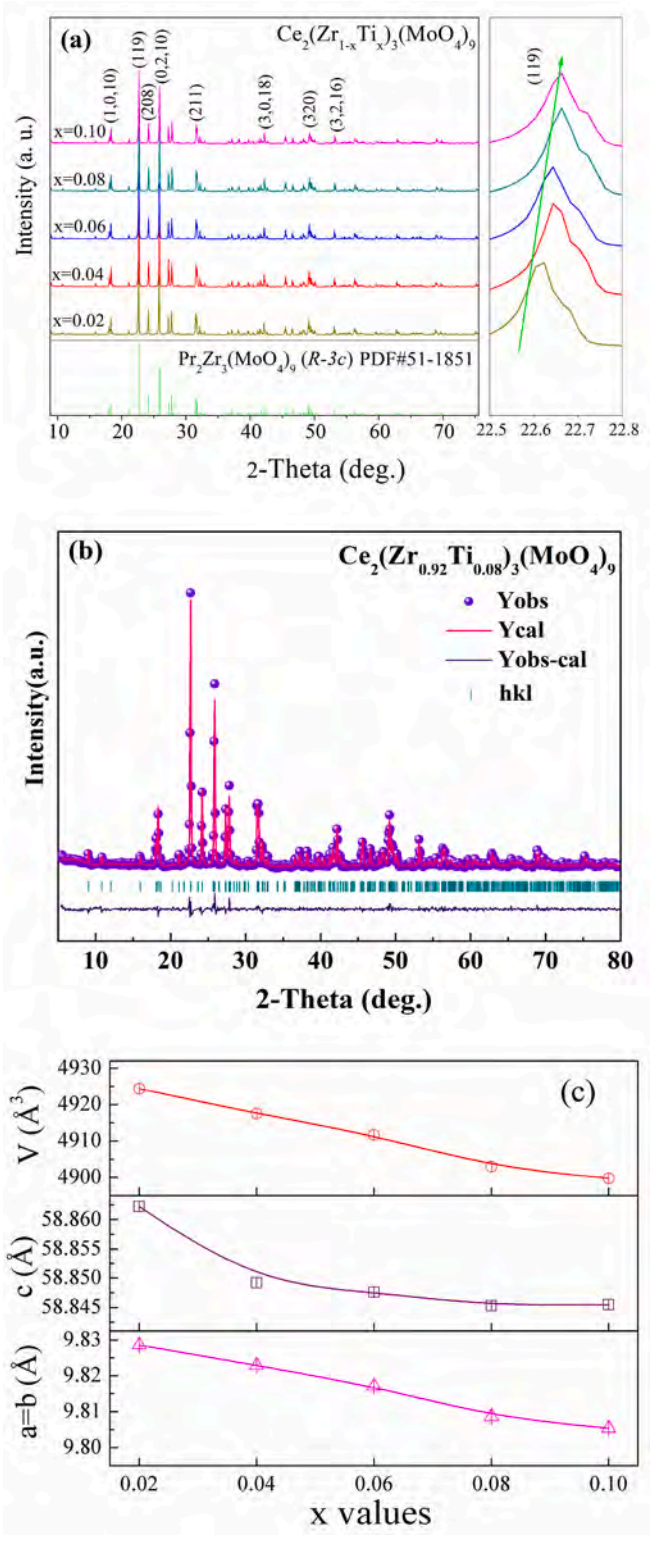

Fig. 1. (a)XRD patterns for $Ce_2(Zr_{1-x}Ti_x)_3(MoO_4)_9$ solid solution; (b)Rietveld refinement plot of $Ce_2(Zr_{0.92}Ti_{0.08})_3(MoO_4)_9$; and (c)Cell parameters of $Ce_2(Zr_{1-x}Ti_x)_3(MoO_4)_9$ as a function of x values.

microwave dielectric properties of $CZ_{1-x}T_xM$ ceramics were systematically discussed as well. Meanwhile, the optimal Ti^{4+} doping content for $CZ_{1-x}T_xM$ ceramics was revealed. Furthermore, the dielectric contributions of optical phonon modes were investigated based on far-infrared reflection spectrum.

Table 1
Crystallographic data obtained from Rietveld refinement of $Ce_2(Zr_{1-x}Ti_x)_3(MoO_4)_9$ ($0.02 \leq x \leq 0.10$) solid solutions.

x	$a = b$ (Å)	c (Å)	V (Å^3)	R_p (%)	R_{wp} (%)
0.02	9.828 (6)	58.862 (2)	4924.3 (9)	6.79	9.51
0.04	9.822 (9)	58.849 (2)	4917.5 (4)	7.01	9.22
0.06	9.817 (1)	58.847 (6)	4911.6 (8)	7.22	9.31
0.08	9.808 (6)	58.845 (3)	4902.9 (8)	6.79	9.51
0.10	9.805 (4)	58.845 (5)	4899.7 (6)	6.77	9.49

2. Experimental procedures

$Ce_2(Zr_{1-x}Ti_x)_3(MoO_4)_9$ ceramics were prepared by solid-state reaction route. High-purity oxide powders of CeO_2, ZrO_2, TiO_2 and MoO_3 mixed according to stoichiometric ratio and then ball-milled with ZrO_2 balls in ethanol medium for 24 h. After drying, the mixtures were calcined at 700 °C for 2 h in atmosphere. The calcined powders were ball-milled and dried again under the same conditions, and then pressed into cylinders of 10 mm × 6 mm size using 10 wt % paraffin wax as a binder. After calcining at 500 °C for 4 h to remove the organics, the bulks were sintered in the temperature range of 650–850 °C in air for 6 h.

The phase composition of $Ce_2(Zr_{1-x}Ti_x)_3(MoO_4)_9$ ceramics was identified by X-ray diffraction (XRD) technique in the 2θ range of 5°–80°. Rietveld refinements were operated to study the structural information of $Ce_2(Zr_{1-x}Ti_x)_3(MoO_4)_9$ ceramics using FullProf software. Scanning electron microscope (SEM, QUANTA FEG250, FEI, USA) and energy dispersive X-ray spectroscopy (EDS) were performed to observe the microstructure and analyze elementary composition, respectively. Infrared reflectivity spectrum was collected by a FT-IR spectrometer (Bruker IFS 66v) at NSRL. Dielectric constant and quality factors in microwave frequencies were evaluated using a network analyzer (N5234A, Agilent Co., USA) in $TE_{01\delta}$ method. A temperature chamber (BPH-120A, Yihengkeji, China) was used to obtain the resonant frequency at 25 °C (f_{25}) and 85 °C (f_{85}). The τ_f values were calculated by the following equation:

$$\tau_f = \frac{f_{85} - f_{25}}{f_{25}(85 - 25)} \times 10^6 (\mathrm{ppm}/^\circ C) \quad (1)$$

3. Results and discussion

Fig. 1(a) shows XRD patterns of $Ce_2(Zr_{1-x}Ti_x)_3(MoO_4)_9$ (x = 0.02–0.10) sintered at the densification temperature for 6 h. A good match could be observed between all the diffraction peaks of as-prepared samples and those of $Pr_2Zr_3(MoO_4)_9$ (JCPDS#51–1851), which's consistent with the $Ce_2Zr_3(MoO_4)_9$ ceramic matrix [25]. Thus, the samples crystallized in the space group *R-3c* (No.167) of the trigonal crystallographic system. It is worth noting that the highest diffraction peaks (119) shift slightly to higher 2θ angles along the increase of Ti-content shown in the figure of locally magnified diffraction peaks near 22°, indicating that the lattice spacing decreases with increasing Ti^{4+} amounts. Rietveld refinement were performed to analyze the crystal structure of $CZ_{1-x}T_xM$ (x = 0.02–0.10) samples, and the typical refined pattern of $Ce_2(Zr_{0.92}Ti_{0.08})_3(MoO_4)_9$ and crystallographic data are presented in Fig. 1(b) and Table 1, respectively. Fig. 1(c) shows the variation of lattice parameters for $Ce_2(Zr_{1-x}Ti_x)_3(MoO_4)_9$ solid solutions. According to Shannon's work, the ionic radius of Ti^{4+} (0.605 Å) at 6 coordinates sites is smaller than that of Zr^{4+} (0.72 Å). Therefore, lattice constants (a, b and c) as well as unit cell volume (V_m) decreased with the increasing of Ti content, which was in agreement with the peak shift of (119) in XRD patterns.

Fig. 2 presents the schematic diagram of $Ce_2Zr_3(MoO_4)_9$ crystal structure for (100) and (001) plane modelled by the DIAMOND software, based on the Crystallographic Information File after XRD refinement. The structural framework consists of three kinds of coordination polyhedra: CeO_9, ZrO_6 and MoO_4, which are connected by sharing

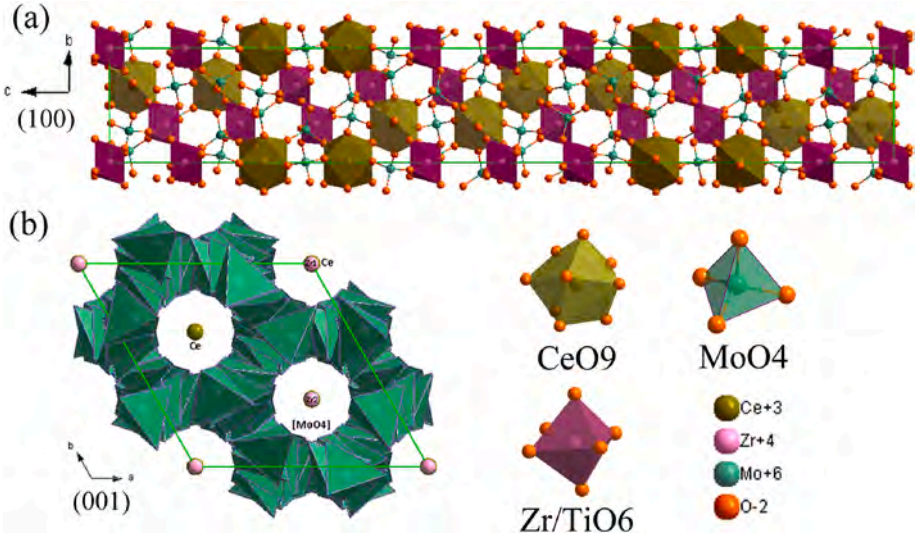

Fig. 2. Schematic illustrating the crystal structure of $Ce_2Zr_3(MoO_4)_9$.

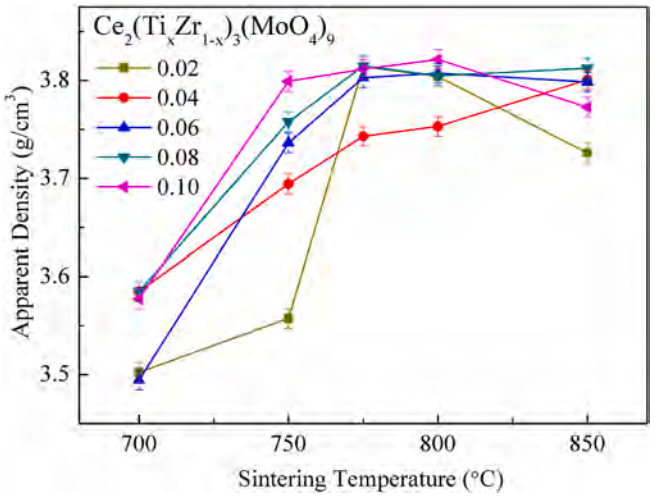

Fig. 3. Apparent densities of $Ce_2(Zr_{1-x}Ti_x)_3(MoO_4)_9$ ($0.02 \leq x \leq 0.10$) solid solution sintered at 700–850 °C.

vertex oxygen atoms with MoO_4 tetrahedron. Both the Ce and Zr ions lie on the threefold axis, while Mo atoms are located on the general position or the twofold axis. Zr atoms have two types of coordination environment at three-dimensional space, in which Zr (1) and Zr (2) atoms occupy the 6b and 12c Wyckoff positions, respectively. When Ti^{4+} is introduced, it would occupy the site of ZrO_6 octahedron.

The apparent densities of ($CZ_{1-x}T_xM$) ($0.02 \leq x \leq 0.1$) ceramics as functions of sintering temperature (700–850 °C) are exhibited in Fig. 3. With increasing sintering temperature, the apparent densities of $Ce_2(Zr_{1-x}Ti_x)_3(MoO_4)_9$ samples rapidly reached their optimum values because of the elimination of pores, and then decreased slightly. Fig. 4 shows the SEM photos of $CZ_{1-x}T_xM$ ($x = 0.02$–0.10) ceramics surfaces sintered at optimum temperatures. Corresponding grain size distributions are shown in the inset of Fig. 4. Clear grain boundaries and few pores were detected in the as-prepared samples. As x values for $CZ_{1-x}T_xM$ ($x = 0.02$–0.10) ceramics increased from 0.02 to 0.08, average grain size increased from 1.82 μm to 3.63 μm. The fact indicated that Ti^{4+} could promote the grain growth in $Ce_2(Zr_{1-x}Ti_x)_3(MoO_4)_9$ ceramics. Fig. 4(f) exhibits the EDX spectra and relative percentage of measured elements for $Ce_2(Zr_{0.92}Ti_{0.08})_3(MoO_4)_9$ ceramic. A small amount of Ti was detected, and the atom molar ratio was close to the stoichiometry of $Ce_2(Zr_{0.92}Ti_{0.08})_3(MoO_4)_9$, which was in accordance with XRD results as shown in Fig. 1.

Fig. 5(a) presents the dielectric constants of specimens with different Ti content and sintering temperature. As the sintering temperature increased, the ε_r values of $CZ_{1-x}T_xM$ ceramics increased up to the optimum values and then decreased slightly. Generally speaking, permittivity depends on intrinsic factors (crystalline structure, ionic polarizability and lattice vibration) and extrinsic factors (pores and impurities). Since the XRD patterns in Fig. 1 demonstrated a single trigonal phase over the whole doping range, relative permittivity of $Ce_2(Zr_{1-x}Ti_x)_3(MoO_4)_9$ was largely affected by the densities at lower temperature range. What's more, permittivity is a function of molecular volume and polarizability according to Clausius-Mossotti equation [34]:

$$\varepsilon_r = \frac{3}{1 - b\alpha_D/V_m} - 2 \tag{2}$$

where b represents a universal constant ($4\pi/3$), α_D is the molecular polarizability, and V_m is the molar volume. By the way, molar volume $V_m = V/Z$ (the values of V have been listed in Table 1, and $Z = 6$). Molecular polarizability α_D could be derived by Shannon additive rule:

$$\alpha_{theo}[Ce_2(Zr_{1-x}Ti_x)_3(MoO_4)_9] = 2\alpha(Ce^{3+}) + 3(1-x)\alpha(Zr^{4+}) + 3(x)\alpha(Ti^{4+}) + 9\alpha(Mo^{6+}) + 36\alpha(O^{2-}) \tag{3}$$

where ionic polarizability has been summarized by Shannon and Choi [35]. It is worth mentioning that α_{theo} $[Ce_2(Zr_{1-x}Ti_x)_3(MoO_4)_9]$ tends to decrease with increasing x values because of the smaller ionic polarizability of Ti^{4+} [$\alpha(Ti^{4+}) = 2.93$ Å^3, $\alpha(Zr^{4+}) = 3.25$ Å^3]. The cell volume (V) also decreased with the increase of Ti^{4+} content as summarized in Table 1. As a result, the ionic polarizability of the primitive unit cell (α_{theo}/V_m) was found to increase from 2.516×10^{-2} at $x = 0.02$ to 2.527×10^{-2} at $x = 0.1$, which was in accordance with the increase of measured permittivity (Fig. 6). Consequently, α_{theo}/V_m also acted as a major affecting factor for dielectric constant.

Fig. 5(b) illustrates the quality factor ($Q{\cdot}f$) of $CZ_{1-x}T_xM$ ($0.02 \leq x \leq 0.1$) ceramics sintered at 700–850 °C for 6 h. As the sintering temperatures increases, the quality factor reached to the maximum value at about 775 °C and then decreased. In particular, the optimal $Q{\cdot}f$ value of $Ce_2(Zr_{0.92}Ti_{0.08})_3(MoO_4)_9$ ceramic was 84,200 GHz, much higher than the $Q{\cdot}f$ value (24,720 GHz) of $Ce_2Zr_3(MoO_4)_9$ matrix reported by Shi. Hence, it is concluded that proper substitution of Ti^{4+} ions could reduce the dielectric loss of the $Ce_2Zr_3(MoO_4)_9$ ceramics. Moreover, it's well

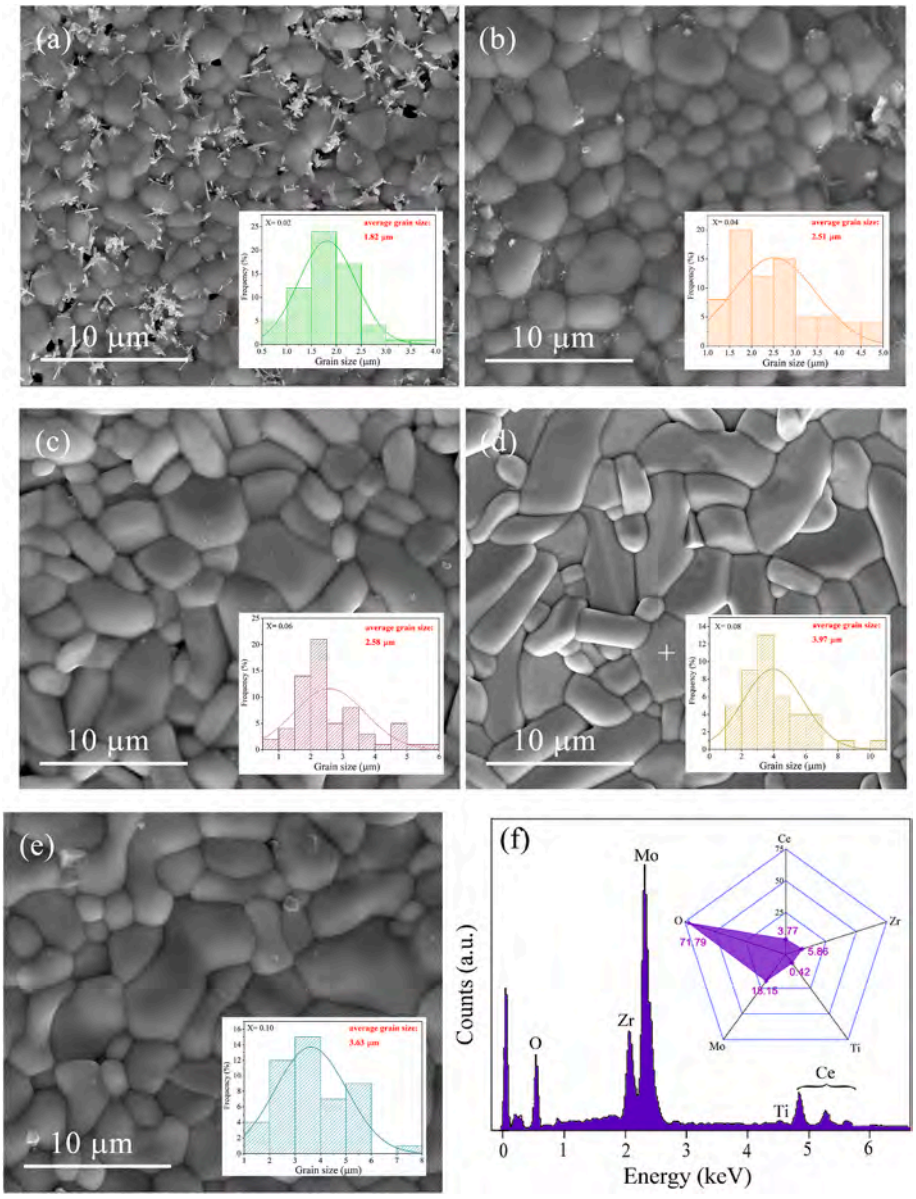

Fig. 4. SEM images and statistics of grain size of the $Ce_2(Zr_{1-x}Ti_x)_3(MoO_4)_9$ ceramics: (a) x = 0.02, (b) x = 0.04, (c) x = 0.06, (d) x = 0.08, (e) x = 0.10 and (f) EDS pattern and element composition for $Ce_2(Zr_{0.02}Ti_{0.08})_3(MoO_4)_9$.

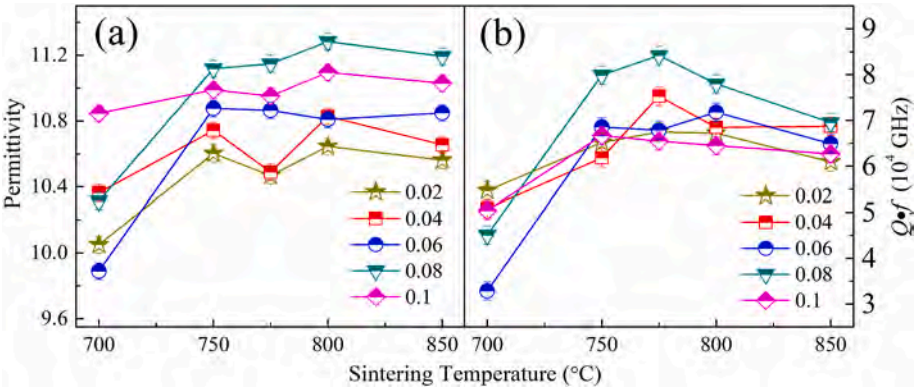

Fig. 5. ε_r and $Q{\cdot}f$ of $Ce_2(Zr_{1-x}Ti_x)_3(MoO_4)_9$ ($0.02 \leq x \leq 0.10$) solid solution sintered at 700–850 °C.

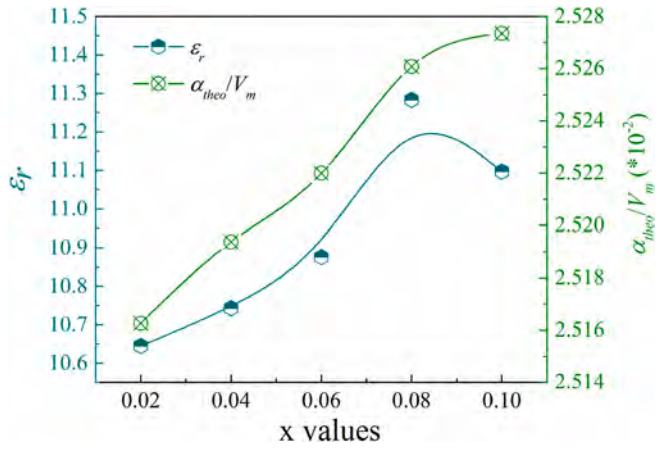

Fig. 6. ε_r and α_{theo}/V_m of $Ce_2(Zr_{1-x}Ti_x)_3(MoO_4)_9$ ceramics as functions of x values.

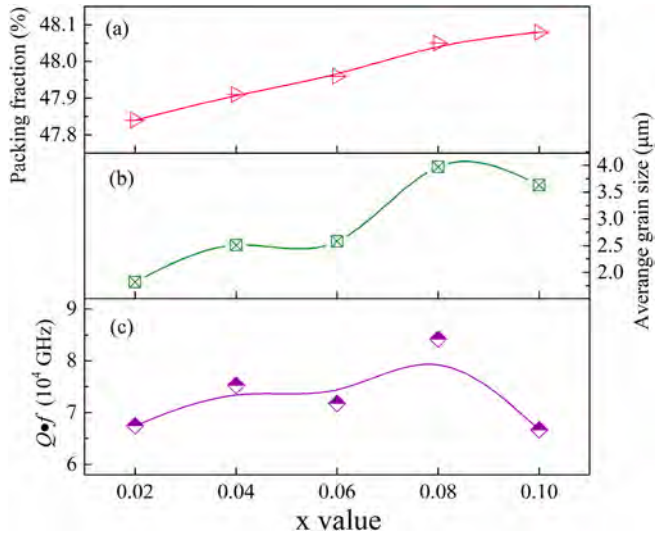

Fig. 7. (a)packing fractions, (b) average grain size, and (c) quality factor of $Ce_2(Zr_{1-x}Ti_x)_3(MoO_4)_9$ ceramics as functions of x values.

known that packing fraction is an essential parameter to correlate the structural evolution with quality factors [29]. The packing fraction is defined as the ratio of the volume for all ions per unit cell to the volume of the cell:

$$\text{Packing Fraction } (\%) = \frac{\text{volume of packed ions}}{\text{volume of unit cell}} \times Z \quad (4)$$

Fig. 7(a) presents the variations of packing fractions as a function of x values for $Ce_2(Zr_{1-x}Ti_x)_3(MoO_4)_9$ ceramics. Since the volume of unit cell decreased with increasing Ti^{4+}-content, the packing fractions of $CZ_{1-x}T_xM$ ceramics showed a gradually increasing trend. It's believed that the increase of the packing fractions lead to the decrease of lattice vibration space, which means the decrease of non-harmonic vibration, thus reducing the intrinsic loss and improving the quality factor. With the increase of Ti^{4+} ion doping, the packing fractions tend to rise, suggesting that packing fractions play a key role in affecting the $Q{\cdot}f$ values in this study. However, the $Q{\cdot}f$ value of $CZ_{1-x}T_xM$ ceramics for x = 0.1 was lower than that of x = 0.08, while the packing fractions was larger than that of x = 0.08, which might be due to the decrease in average grain sizes. As the microwave propagates in the medium, it will refract and reflect at the grain boundaries. The decrease of grain sizes will result in increased number of reflection of microwave at the grain boundaries, and hence increased transmission path of the microwave in the medium

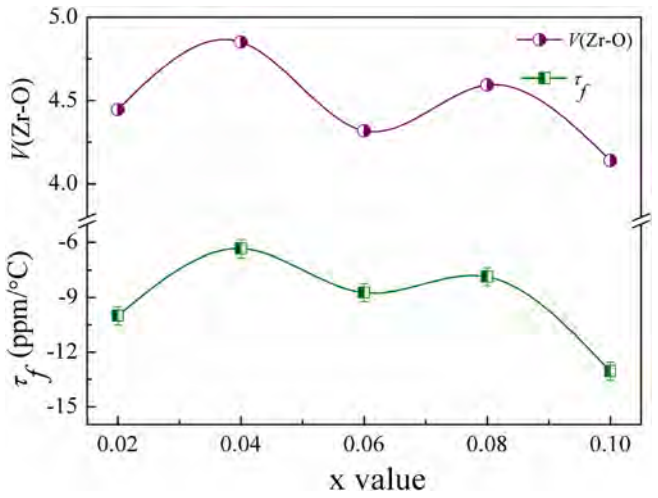

Fig. 8. The variation of τ_f values and the Zr-site bond valence *V(Zr-O)* of $Ce_2(Zr_{1-x}Ti_x)_3(MoO_4)_9$ ceramics with x values.

and increased loss of interaction between microwave and the medium, i.e., reduced quality factor [36–38]. The dependence $Q{\cdot}f$ values of $Ce_2(Zr_{1-x}Ti_x)_3(MoO_4)_9$ ceramics as function of x values had similar trend to the change in average grain sizes in this work as plotted in Fig. 7. Accordingly, the highest $Q{\cdot}f$ value (84,200 GHz) was obtained at x = 0.08 for $Ce_2(Zr_{1-x}Ti_x)_3(MoO_4)_9$ ceramics.

Fig. 8 plots the curve of τ_f over x values. The τ_f values fluctuated between −13 and −6 ppm/°C with the change of Ti^{4+} doping content. In relevant reports [39], the τ_f value is sensitive to the bond valence (*Vi*), a parameter related to the bond lengths, and the calculation equation of V_i is as follows:

$$V_i = \sum_j v_{ij} \quad (5)$$

$$v_{ij} = \exp\left(\frac{R_{ij} - d_{ij}}{b'}\right) \quad (6)$$

where R_{ij} is the bond valence parameter between atoms j and i. Based on Brown and Altermatt's work [40], bond valence parameters R_{ZrO} = 1.928 Å and R_{TiO} = 1.815 Å. d_{ij} is the bond length, which could be obtained by Rietveld structural refinements. b' is considered to be a

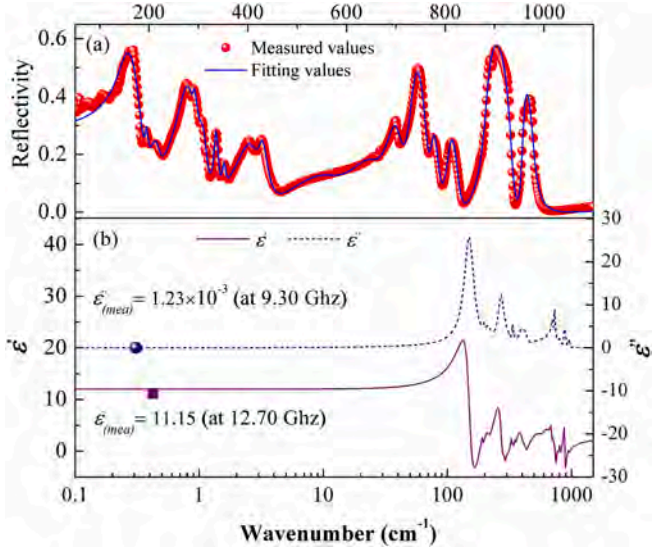

Fig. 9. (a) Measured and fitted IR spectra, (b) the real and imaginary part of the complex dielectric function of $Ce_2(Zr_{0.92}Ti_{0.08})_3(MoO_4)_9$ ceramic.

Table 2
Fitting parameters of IR spectrum for $Ce_2(Zr_{0.02}Ti_{0.08})_3(MoO_4)_9$ ceramic.

$Ce_2(Zr_{0.02}Ti_{0.08})_3(MoO_4)_9$			$\varepsilon_0 = 12.01$	$\varepsilon_\infty = 2.60$
Mode	ω_{oj}	ω_{pj}	γ_j	$\Delta\varepsilon_j$
1	150.38	354.26	33.06	5.55
2	194.14	50.80	23.45	0.07
3	213.14	115.22	23.46	0.29
4	271.25	320.20	32.60	1.39
5	289.80	62.38	8.05	0.05
6	305.72	86.49	17.57	0.08
7	334.11	96.15	7.72	0.08
8	351.69	59.54	7.42	0.03
9	399.95	290.70	52.52	0.53
10	426.21	105.63	16.86	0.06
11	557.60	317.69	118.35	0.32
12	645.67	300.04	66.28	0.22
13	695.04	347.48	32.97	0.25
14	732.41	335.05	20.90	0.21
15	773.30	136.64	16.32	0.03
16	807.42	193.19	19.80	0.06
17	883.49	360.29	17.65	0.17
18	955.34	138.78	10.69	0.02

constant (0.37 Å). The bigger bond valence means bigger the restoring force for the tilting recovery and more stable crystal structure, and this cause better temperature stability. In this case, the bond valence of Zr site changes as the substitution of Ti^{4+} for Zr^{4+}, and the calculated results of V_{Zr} are shown in Fig. 8. The variation tendency of τ_f was similar to bond valence, suggesting the strong dependence on bond valence.

In order to study the intrinsic dielectric constant and loss, far-infrared reflectance spectrum of $Ce_2(Zr_{0.92}Ti_{0.08})_3(MoO_4)_9$ ceramic has been analyzed based on the Lorentz model, in which $\varepsilon^*(\omega)$ is the summation of optical dielectric constant (ε_∞) and dielectric constant contributed by each vibration mode:

$$\varepsilon^*(\omega) = \varepsilon_\infty + \sum_{j=1}^{n} \frac{\omega_{pj^2}}{\omega_{oj^2} - \omega^2 - j\gamma_j\omega} \tag{7}$$

where $\varepsilon^*(\omega)$ represents the complex dielectric function; n is the number of resonant modes; and γj, ω_{oj} and ω_{pj} denotes the damping constant, the transverse frequency, and plasma frequency of the *j*th polar vibration modes, respectively. The relationship between complex reflectivity $R(\omega)$ and permittivity can expressed as:

$$R(\omega) = \left|\frac{1 - \sqrt{\varepsilon^*(\omega)}}{1 + \sqrt{\varepsilon^*(\omega)}}\right|^2 \tag{8}$$

Fig. 9 shows the fitted infrared reflectivity spectra and calculated complex dielectric spectra of $Ce_2(Zr_{0.92}Ti_{0.08})_3(MoO_4)_9$ compound in the 50-1200 cm^{-1} wavenumber range. The phonon parameters of the $Ce_2(Zr_{0.92}Ti_{0.08})_3(MoO_4)_9$ ceramic obtained from fitting by Reffit software are listed in Table 2. There were 18 resonant modes for $Ce_2(Zr_{0.92}Ti_{0.08})_3(MoO_4)_9$ ceramic and the ε_∞ was 2.60. The measured dielectric constant (11.15) was equal to that of calculated value (12.01), and the slight differences may be due to the presence of extrinsic defects. Meanwhile, the measured dielectric loss (ε'') was on the same order of magnitude as the calculated value, indicating that the vibration modes at infrared regions contributed to the polarization response for $Ce_2(Zr_{0.92}Ti_{0.08})_3(MoO_4)_9$ ceramic at the microwave frequencies.

4. Conclusion

In this work, $Ce_2(Zr_{1-x}Ti_x)_3(MoO_4)_9$ (x = 0.02–0.1) ceramics were prepared via the traditional solid-state method. The influences of the substitution of a small amount Ti^{4+} for Zr^{4+} on the phase composition, sintering behavior, microstructure and microwave dielectric properties of $Ce_2Zr_3(MoO_4)_9$ ceramics were systematically investigated. A single trigonal phase *R-3c* (NO.167) was achieved in the whole composition range of $0.02 \leq x \leq 0.10$, which was determined by means of X-ray powder diffraction and confirmed by Rietveld refinements. Packing fraction combined with average grain size could explain the variation of quality factor. Permittivity was mainly related to the ionic polarizability of the primitive unit cell, and the τ_f value was positively correlated to the bond valence. Moreover, far-infrared spectrum demonstrated that the major polarization contribution of $Ce_2(Zr_{0.92}Ti_{0.08})_3(MoO_4)_9$ ceramics at microwave frequency was due to the absorption of structural phonon oscillation. The optimum microwave dielectric properties were obtained in the $Ce_2(Zr_{0.92}Ti_{0.08})_3(MoO_4)_9$ with a ε_r of 11.28, a high $Q{\cdot}f$ of 84,200 GHz and a near zero τ_f of −7.86 ppm/°C.

Declaration of competing interest

The authors declare that they have no known competing financial interests or personal relationships that could have appeared to influence the work reported in this paper.

Acknowledgements

This work was supported by the National Natural Science Foundation of China (No. 51972143). The authors are also thankful to the administrators in IR beamline workstation of National Synchrotron Radiation Laboratory (NSRL) for the help in IR measurement.

References

[1] M.T. Sebastian, R. Ubic, H. Jantunen, Low-loss dielectric ceramic materials and their properties, Int. Mater. Rev. 60 (2015) 392–412, https://doi.org/10.1179/1743280415Y.0000000007.
[2] H.I. Hsiang, C.C. Chen, S.Y. Yang, Microwave dielectric properties of $Ca_{0.7}Nd_{0.2}TiO_3$ ceramic-filled CaO-B_2O_3-SiO_2 glass for LTCC applications, J. Adv. Ceram. 8 (2019) 345–351, https://doi.org/10.1007/s40145-019-0316-6.
[3] J.M. Li, C.M. Zhang, H. Liu, T. Qiu, C.G. Fan, Structure, morphology, and microwave dielectric properties of $SmAlO_3$ synthesized by stearic acid route, J. Adv. Ceram. (2020), https://doi.org/10.1007/s40145-020-0394-5.
[4] H.C. Xiang, C.C. Li, H. Jantunen, L. Fang, A.E. Hill, Ultralow loss $CaMgGeO_4$ microwave dielectric ceramic and its chemical compatibility with silver electrodes for low-temperature cofired ceramic applications, ACS Sustain. Chem. Eng. 6 (2018) 6458–6466, https://doi.org/10.1021/acssuschemeng.8b00220.
[5] C.X. Su, L.Y. Ao, Z.W. Zhang, Y.F. Zhai, J.Q. Chen, Y. Tang, L.J. Liu, L. Fang, Crystal structure, Raman spectra and microwave dielectric properties of novel temperature-stable $LiYbSiO_4$ ceramics, Ceram. Int. 46 (2020) 19996–20003, https://doi.org/10.1016/j.ceramint.2020.05.070.
[6] J.X. Bi, C.F. Xing, C.H. Yang, H.T. Wu, Phase composition, microstructure and microwave dielectric properties of rock salt structured Li_2ZrO_3-MgO ceramics, J. Eur. Ceram. Soc. 38 (2018) 3840–3846, https://doi.org/10.1016/j.jeurceramsoc.2018.04.034.
[7] Z.W. Zhang, L. Fang, H.C. Xiang, M.Y. Xu, Y. Tang, H. Jantunen, C.C. Li, Structural, infrared reflectivity spectra and microwave dielectric properties of the $Li_7Ti_3O_9F$ ceramic, Ceram. Int. 45 (2019) 10163–10169, https://doi.org/10.1016/j.ceramint.2019.02.065.
[8] M.Y. Yu, Y. Tang, J. Li, W.S. Fang, L. Duan, L. Fang, Microwave dielectric properties and chemical compatibility with alumina electrode of two novel ultra-low temperature firing $ATeMoO_6$ (A = Mg, Zn) ceramics, Ceram. Int. 46 (2020) 25619–25625, https://doi.org/10.1016/j.ceramint.2020.07.036.
[9] C.Z. Yin, C.C. Li, G.J. Yang, L. Fang, Y.H. Yuan, L.L. Shu, J.B. Khaliq, $NaCa_4V_5O_{17}$: a low-firing microwave dielectric ceramic with low permittivity and chemical compatibility with silver for LTCC applications, J. Eur. Ceram. Soc. 40 (2020) 386–390, https://doi.org/10.1016/j.jeurceramsoc.2019.09.029.
[10] J.J. Zheng, Y.K. Yang, H.T. Wu, Y.Y. Zhou, Z.L. Zhang, Structure, infrared spectra and microwave dielectric properties of the novel Eu_2TiO_5 ceramics, J. Am. Ceram. Soc. 103 (2020) 4333–4341, https://doi.org/10.1111/jace.17092.
[11] Y. Tang, M.Y. Yu, Z.W. Zhang, J.Q. Chen, H.C. Xiang, X.R. Xing, L. Fang, A novel tungstate $Li_3Nd_3W_2O_{12}$ with garnet structure for low-temperature cofired ceramic technology, J. Eur. Ceram. Soc. 40 (2020) 1386–1389, https://doi.org/10.1016/j.jeurceramsoc.2019.11.083.
[12] L.X. Pang, D. Zhou, Modification of $NdNbO_4$ microwave dielectric ceramic by Bi substitutions, J. Am. Ceram. Soc. 102 (2019) 2278–2282, https://doi.org/10.1111/jace.16290.
[13] F.Y. Huang, H. Su, Y.X. Li, H.W. Zhang, X.L. Tang, Low-temperature sintering and microwave dielectric properties of $CaMg_{1-x}Li_{2x}Si_2O_6$ (x = 0−0.3) ceramics, J. Adv. Ceram. 9 (2020) 471–480, https://doi.org/10.1007/s40145-020-0390-9.
[14] H.H. Guo, D. Zhou, W.F. Liu, L.X. Pang, D.W. Wang, J.Z. Su, Z.M. Qi, Microwave dielectric properties of temperature-stable zircon-type (Bi, Ce)VO_4 solid solution ceramics, J. Am. Ceram. Soc. 103 (2020) 423–432, https://doi.org/10.1111/jace.16759.

[15] X.L. Chen, X. Li, H.F. Zhou, J. Sun, X.X. Li, X. Yan, C.C. Sun, J.P. Shi, Phase evolution, microstructure, electric properties of $(Ba_{1-x}Bi_{0.67x}Na_{0.33x})(Ti_{1-x}Bi_{0.33x}Sn_{0.67x})O_3$ ceramics, J. Adv. Ceram. 8 (2019) 427–437, https://doi.org/10.1007/s40145-019-0326-4.

[16] M.J. Wu, Y.C. Zhang, M.Q. Xiang, Synthesis, characterization and dielectric properties of a novel temperature stable (1-x)$CoTiNb_2O_8$-x$ZnNb_2O_6$ ceramic, J. Adv. Ceram. 8 (2019) 228–237, https://doi.org/10.1007/s40145-018-0308-y.

[17] S.Z. Hao, D. Zhou, F. Hussain, W.F. Liu, J.Z. Su, D.W. Wang, Q.P. Wang, Z.M. Qi, C. Singh, S. Trukhanov, Structure, spectral analysis and microwave dielectric properties of novel x$(NaBi)_{0.5}MoO_4$-(1-x)$Bi_{2/3}MoO_4$ (x = 0.2-0.8) ceramics with low sintering temperatures, J. Eur. Ceram. Soc. 40 (2020) 3569–3576, https://doi.org/10.1016/j.jeurceramsoc.2020.03.074.

[18] Z.W. Zhang, Y. Tang, J. Li, J.Q. Chen, A.H. Yang, Y. Wang, Y.F. Zhai, L.Y. Ao, C. X. Su, X.R. Xing, L. Fang, High-*Q* and near-zero τ_f composite $Li_2Mg_2TiO_5$-$Sr_3(VO_4)_2$ ceramics for low-temperature co-fired ceramic applications, Ceram. Int. 46 (2020) 8281–8286, https://doi.org/10.1016/j.ceramint.2019.12.057.

[19] W.J. Bian, X.C. Lu, Y. Wang, H.K. Zhu, T. Chen, S.W. Ta, Q.T. Zhang, Correlations between structure and microwave dielectric properties of Co doped $MgMoO_4$ ceramics, Ceram. Int. 46 (2020) 22024–22029, https://doi.org/10.1016/j.ceramint.2020.05.187.

[20] J. Dhanya, A.V. Basiluddeen, R. Ratheesh, Synthesis of ultra low temperature sinterable $Na_2Zn_5(MoO_4)_6$ ceramics and the effect of microstructure on microwave dielectric properties, Scripta Mater. 132 (2017) 1–4, https://doi.org/10.1016/j.scriptamat.2017.01.017.

[21] H.H. Guo, D. Zhou, L.X. Pang, Z.M. Qi, Microwave dielectric properties of low firing temperature stable scheelite structured (Ca, Bi)(Mo, V)O_4 solid solution ceramics for LTCC applications, J. Eur. Ceram. Soc. 39 (2019) 2365–2373, https://doi.org/10.1016/j.jeurceramsoc.2019.02.010.

[22] S.Z. Hao, D. Zhou, F. Hussain, J.Z. Su, W.F. Liu, D.W. Wang, Q.P. Wang, Z.M. Qi, Novel scheelite-type $[Ca_{0.55}(Nd_{1-x}Bi_x)_{0.3}]MoO_4$ ($0.2 \leq x \leq 0.95$) microwave dielectric ceramics with low sintering temperature, J. Am. Ceram. Soc.. https://doi.org/10.1111/jace.17378.

[23] J.G. Bazarova, Y.L. Tushinova, B.G. Bazarov, S.G. Dorzhieva, Double molybdates of rare earth elements and zirconium, Russ. Chem. Bull. 66 (2017) 587–592, https://doi.org/10.1007/s11172-017-1777-9.

[24] W.Q. Liu, R.Z. Zuo, A novel low-temperature firable $La_2Zr_3(MoO_4)_9$ microwave dielectric ceramic, J. Eur. Ceram. Soc. 38 (2018) 339–342, https://doi.org/10.1016/j.jeurceramsoc.2017.08.023.

[25] L. Shi, C. Liu, H.W. Zhang, R. Peng, G. Wang, X.L. Shi, X.Y. Wang, W.W. Wang, Crystal structure, Raman spectroscopy, metal compatibility and microwave dielectric properties of $Ce_2Zr_3(MoO_4)_9$ ceramics, Mater. Chem. Phys. 250 (2020) 122954, https://doi.org/10.1016/j.matchemphys.2020.122954.

[26] B.J. Tao, C.F. Xing, W.F. Wang, H.T. Wu, Y.Y. Zhou, A novel $Ce_2Zr_3(MoO_4)_9$ microwave dielectric ceramic with ultra-low firing temperature, Ceram. Int. 45 (2019) 24675–24683, https://doi.org/10.1016/j.ceramint.2019.08.206.

[27] W.Q. Liu, R.Z. Zuo, Low temperature fired $Ln_2Zr_3(MoO_4)_9$ (Ln = Sm, Nd) microwave dielectric ceramics, Ceram. Int. 43 (2017) 17229–17232, https://doi.org/10.1016/j.ceramint.2017.09.083.

[28] Y.H. Zhang, J.J. Sun, N. Dai, Z.C. Wu, H.T. Wu, C.H. Yang, Crystal structure, infrared spectra and microwave dielectric properties of novel extra low-temperature fired $Eu_2Zr_3(MoO_4)_9$ ceramics, J. Eur. Ceram. Soc. 39 (2019) 1127–1131, https://doi.org/10.1016/j.jeurceramsoc.2018.12.042.

[29] Y.H. Zhang, H.T. Wu, Crystal structure and microwave dielectric properties of $La_2(Zr_{1-x}Ti_x)3(MoO_4)_9$ ($0 \leq x \leq 0.1$) ceramics, J. Am. Ceram. Soc. 102 (2019) 4092–4102, https://doi.org/10.1111/jace.16268.

[30] H. Li, X. Chen, Q. Xiang, B. Tang, J. Lu, Y. Zou, S. Zhang, Structure, bond characteristics and Raman spectra of $CaMg_{1-x}Mn_xSi_2O_6$ microwave dielectric ceramics, Ceram. Int. 45 (2019) 14160–14166, https://doi.org/10.1016/j.ceramint.2019.04.117.

[31] H.H. Guo, D. Zhou, C. Du, P.J. Wang, W.F. Liu, L.X. Pang, Q.P. Wang, J.Z. Su, C. Singh, S. Trukhanov, Temperature stable $Li_2Ti_{0.75}(Mg_{1/3}Nb_{2/3})_{0.25}O_3$-based microwave dielectric ceramics with low sintering temperature and ultra-low dielectric loss for dielectric resonator antenna applications, J. Mater. Chem. C. 8 (2020) 4690–4700, https://doi.org/10.1039/D0TC00326C.

[32] R.D. Shannon, Revised effective ionic radii and systematic studies of interatomic distances in halides and chalcogenides, Acta Crystallogr. A32 (1976) 751–767, https://doi.org/10.1107/S0567739476001551.

[33] A. Ullah, H.X. Liu, H. Hao, J. Lqbal, Z.H. Yao, M.H. Cao, Influence of TiO_2 additive on sintering temperature and microwave dielectric properties of $Mg_{0.9}Ni_{0.1}SiO_3$ ceramics, J. Eur. Ceram. Soc. 37 (2017) 3045–3049, https://doi.org/10.1016/j.jeurceramsoc.2017.03.047.

[34] A.J. Bosman, E.E. Havinga, Temperature dependence of dielectric constants of cubic ionic compounds, Phys. Rev. 129 (1963) 1593–1600, https://doi.org/10.1103/PhysRev.129.1593.

[35] R.D. Shannon, Dielectric polarizabilities of ions in oxides and fluorides, J. Appl. Phys. 73 (1993) 348–366, https://doi.org/10.1063/1.353856.

[36] J. Perm, N.M. Alford, A. Templeton, X.R. Wang, M.S. Xu, M. Reece, K. Schrapel, Effect of porosity and grain size on the microwave dielectric properties of sintered alumina, J. Am. Ceram. Soc. 80 (2005) 1885–1888, https://doi.org/10.1111/j.1151-2916.1997.tb03066.x.

[37] P. Zhang, H. Xie, Y.G. Zhao, M. Xiao, Synthesis and microwave dielectric characteristics of high-Q $Li_2Mg_xTiO_{3+x}$ ceramics system, Mater. Res. Bull. 98 (2018) 160–165, https://doi.org/10.1016/j.materresbull.2017.10.012.

[38] J.Y. Hao, J. Guo, E. Zhao, M.M. Si, X.F. Yuan, F.Z. Yao, H. Wang, Grain size effect on microwave dielectric properties of Na_2WO_4 ceramics prepared by cold sintering process Ceram. Int. https://doi.org/10.1016/j.ceramint.2020.07.200.

[39] N.E. Brese, M. O'Keeffe, Bond-valence parameters for solids, Acta Crystallogr. B47 (1991) 192–197, https://doi.org/10.1107/S0108768190011041.

[40] I.D. Brown, D. Altermatt, Bond-valence parameters obtained from a systematic analysis of the inorganic crystal structure database, Acta Crystallogr. B41 (1985) 244–247, https://doi.org/10.1107/S0108768185002063.